Approximate Evaluation of Slender Radome Performance in Hypersonic Flight

FRANK A ALBINI*
Hughes Aircraft Company, El Segundo, Calif

General considerations concerning the material and shape of a hypersonic radome reveal a series of unifying physical restrictions on such structures The aerodynamics of such shapes at hypersonic speeds admits of unifying simplification as well, for the entropy layer and the highly ionized region of flow are nearly coincident A computational procedure is outlined which provides an approximate map of the entropy layer density, temperature, etc , for flow fields in which thermochemical equilibrium is maintained Using these data to generate a dielectric constant profile completes the specification of the electromagnetic problem This portion of the problem is attacked on an approximate basis, which is expected to be more accurate than ray-tracing, since the interaction zone should be of the order of a wavelength in dimension Interpretation of the results in terms of boresight-error-limited and power-limited trajectories is discussed cursorily, and appendices illustrate implementation of the calculations by digital computer

Nomenclature

a = speed of sound
a,b,c,d = constants used in Appendix B [see Eqs (B3–B6)]
C_p = pressure coefficient = $[2(P - P_\infty)/\rho_\infty u_\infty^2]$
D_b = body nose diameter
$\mathbf{e}$ = unit vector in s direction
$\mathbf{E}$ = electric field intensity
f,g,F,G = dummy functions
$\mathbf{H}$ = magnetic field intensity
H_f = dimensionless enthalpy function
h = specific enthalpy
i = imaginary unit = $-1^{1/2}$
K = dielectric constant
k_0 = wave number of electromagnetic wave
M = Mach number
m = electron mass
N = electron concentration
P = pressure
Q_j = $(K_j - \sin^2\theta)^{1/2}$
q = electron charge
r_i = distance from vehicle centerline to ith streamline normal to local body surface
R = gas constant
$R_{1\,2}$ = voltage reflection coefficient for polarization 1,2
r = radius, cylindrical coordinates, to shock wave
S_R = dimensionless specific entropy
T = temperature, °K
$T_{1\,2}$ = voltage transmission coefficient for polarization 1,2
u = velocity, also dummy variable in Appendix B
x,y,z = Cartesian coordinates defined variously in text
Z = compressibility factor
$\alpha_n,\beta_n,\gamma_n,\delta_n$ = coefficients used in Appendix B, Eq (B8) ff
α = angle of polarization of electromagnetic wave
γ_{ij} = $\exp(ik_0 Q_i z_j)$
γ = isentropic exponent
ϵ_0 = permittivity of vacuum
μ_0 = permeability of vacuum
ν = electron collision-damping frequency
ρ = mass density
θ = angle of incidence of electromagnetic wave
ω = electromagnetic wave circular frequency
ω_p = Lorentz plasma frequency

Subscripts

1,2 = initial, final flow conditions
i = index number on a streamline
b = body surface
s = shock wave
∞ = freestream

Received August 5, 1963; revision received December 24, 1963 This work was supported in part by Advanced Research Projects Agency Contract DA 04 495-AMC 3Z, Advanced Research Projects Agency Order 337-62 The author gratefully acknowledges many informative discussions with J K Yakura pertaining to the aerodynamic calculations, and thanks G S Campbell for his helpful criticism of the manuscript

* Member Technical Staff, Space Systems Division Present address: Institute for Defense Analyses, Washington, D C Member AIAA

Introduction

THE study of hypersonic, guided flight entails the analysis of a broad range of engineering problems, including heat transfer, aerodynamic and structural stability, control processes, and guidance implementation In addition to the difficulties associated with heat transfer, mechanical strength, and aerodynamic shaping, the radome designer must consider a new problem: the influence of the ionization layer on the electromagnetic signal to be passed It is the purpose of the present work to outline some basic considerations in this particular area, to discuss some usually admissible simplifications, and to detail a computational procedure that will implement the analysis of this class of problems

General Considerations

In general, hypersonic flight of other than re-entry vehicles precludes the use of blunted shapes The forebodies of most hypersonic vehicles will therefore be slender However, from thermal considerations it will also usually be required that there be some bluntness of the tip of the body, particularly when radome materials are employed at the tip Because the radome cannot operate effectively if the thickness of it changes appreciably during flight, it will probably be made of refractory rather than ablative materials Also, ablation to any large extent may introduce impurities into the boundary layer which are easily ionized, thus perhaps degrading the radome performance

The thickness of the radome material is ordinarily selected to minimize the loss of power and reduce phase distortion to a minimum and, as such, will generally be of the order of one-half wavelength (measured in the material) thick Wavelengths presently employed which are contemplated for development fall in the 1–10 cm region, since lower frequencies entail microwave "plumbing" penalties and higher

frequencies begin to suffer atmospheric attenuation Achievement of reasonable antenna gain ($\gtrsim 20$ db) requires, then, a radome base diameter in the neighborhood of 5–50 cm to house the necessary aperture Aerodynamic slenderness then requires a length of 15–150 cm, and blunting requirements thus imply a nose radius on the order of 1–10 cm

If the structural observations just mentioned are admitted, it appears that the hypersonic radome is roughly outlined aerodynamically on a wavelength scale Therefore, the remaining parameters are Mach number and altitude, which, when fixed, determine the flow field, including ionization levels With the wavelength, electron concentration, and collision-damping frequency determined, the electromagnetic interaction is determined by the direction of wave propagation Therefore, in a general way, it can be stated that the hypersonic radome performance should be estimable by uniformly applicable approximate procedures The simplifying assumptions pertinent to these approximations are discussed below, the computational methods are outlined in general, and the resulting procedures are discussed in terms of mechanized computations in the appendices

Aerodynamic Approximations

The analysis of the flow field of a slender, blunted body in hypersonic flight has been the subject of extensive investigation [1] For present purposes what is required is a fairly accurate map of that region of inviscid flow that is sufficiently hot to be ionized to a significant level † This zone is roughly that region of the flow that has passed through the bow shock wave at a distance of the order of the blunt nose radius from the vehicle axis of symmetry This region is characterized by a steep entropy gradient normal to the body surface and has been labeled the "entropy layer "[3] An important characteristic of the entropy layer is that, to first order,[3] it is at constant pressure

If the entropy layer is assumed to be at constant pressure, then the specification of the pressure on the body surface and the entropy along a streamline suffice to determine the thermodynamic state on the streamline at that body location under the assumptions of thermochemical equilibrium‡ and isentropic flow behind the shock wave Thus, the need is for an expression for the shock-wave position and a means of estimating body pressure For the shape of the shock wave, correlation studies have provided a semiempirical expression[4] of the form

$$r/D_b = k(x/D_b)^n \tag{1}$$

The adjustable constants k and n are given in terms of Mach number in Ref 4 and in the range $8 \leq M_\infty \leq 20$ can be fitted by

$$k \approx 1\ 273\text{–}0\ 0167M_\infty \tag{2}$$

$$n \approx 0\ 469\text{–}0\ 00125M_\infty \tag{3}$$

From these formulas the inclination angle of the shock in terms of radial position is given by

$$\theta_s \approx \tan^{-1}[nk^{-1/n}(r/D_b)^{n-1/n}] \tag{4}$$

With these approximate forms, the conditions behind the shock wave are readily estimated for any streamline within the entropy layer zone by reference to equilibrium air shock wave tables[5] or iterative computation (see Appendix A)

The pressure on the surface of the body can be estimated for high Mach number (≥ 8) and sufficiently large local body slope ($>10°$) by the simple Newtonian flow theory adjusted semiempirically [6] Newtonian theory gives a local pressure coefficient

$$C_p = 2\sin^2\theta_b \tag{5}$$

which better fits experimental data if reduced by one-half the stagnation pressure coefficient, or about 8% for air at high Mach number The result is a pressure distribution:

$$P_b/P_\infty \doteq 1 + 1\ 29M_\infty^2 \sin^2\theta_b \tag{6}$$

Using this pressure distribution and the entropy behind the shock wave, reference to an air chart[7] provides thermodynamic conditions along any chosen streamline (any r/D_b) in the entropy layer The location r_i of a streamline i is determined by satisfying the equations of continuity and energy conservation simultaneously[8] and proceeding stepwise between streamlines, using average values for the mass flux ρu:

$$\tfrac{1}{2}u_i^2 + h_i = \tfrac{1}{2}u_\infty^2 + h_\infty \tag{7}$$

$$\rho_\infty u_\infty(r_{i+1}^2 - r_i^2) = 2\int_{r_i}^{r_{i+1}} \rho u r dr \approx \overline{(\rho u)}_{i\ i+1}(r_{i+1}^2 - r_i^2) \tag{8}$$

Therefore, by selecting a mesh of streamlines ahead of the shock wave (r_i) and processing them along the body pressure distribution in the manner outlined, a map of density and temperature in the entropy layer is obtained Reference to air composition tables or charts then provides the electron concentration N from which the plasma frequency ω_p is obtained:

$$\omega_p = (Nq^2/m\epsilon_0)^{1/2} \approx 5\ 65 \times 10^4 N^{1/2}\ \text{sec}^{-1} \qquad N \text{ in cc}^{-1} \tag{9}$$

The collision damping frequency ν may be estimated crudely by

$$\nu \doteq 2 \times 10^{10}\ T^{1/2}\rho/\rho_0\ \text{sec}^{-1} \qquad \rho_0 = 1\ 29\ \text{g/liter} \tag{10}$$

or constructed more accurately by computation (for example, as outlined in Ref 9) Examination of results of these computations will show that ν_c is well approximated by a constant in many cases § These parameters characterize the zone electrically, since the equivalent dielectric constant for a wave of circular frequency ω is given by

$$K = 1 - (\omega_p/\omega)^2/(1 + i\nu/\omega) \tag{11}$$

The mechanization of the forementioned computations for digital computer application is made possible by the use of thermodynamic functions for equilibrium air expressed explicitly in terms of P and ρ[10] as discussed in Appendix A

Electromagnetic Approximations

As is well known in the field, the calculation of radome performance (even without ionization layer) is an unrewarding effort at best The difficulty arises from the near-zone nature of the radome/antenna interaction and the complex shape of each Asymptotic methods, such as ray-tracing and plane slab assumptions can provide qualitative data, but recourse to experimentation usually is made to obtain boresight errors or similar precise data

In light of this fact there seems to be little virtue in formulating the general problem, but engineering-accuracy ap-

† If the boundary-layer thickness is greater than $\sim 0\ 1$ wavelength, then the electron concentration variation across it should be considered [12, 13] Estimated boundary layer thickness by the method of Deissler and Loeffler[2] seems to fall below this thickness for typical conditions of this study, although a significant effect was anticipated by Swift and Evans[11] for a higher altitude case The refractory radome surface is assumed here not to influence the electron concentration distribution, a question not fully settled yet

‡ For the nose radii under consideration here and for altitudes below 100,000 ft, this assumption should be acceptable below $M_\infty = 20$

§ If the boundary layer need be considered, the collision frequency can probably be assumed constant through this region as well (cf Ref 11)

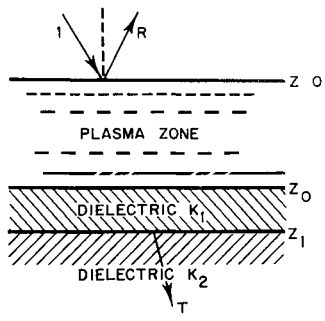

Fig 1a Geometry of the incident wave problem

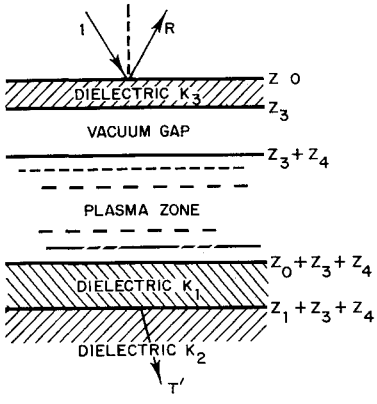

Fig 1b Artificial problem employed to approximate emergent wave case

proximation should be sought The approximation suggested rests on a comparison between the results of computations with and without the ionization sheath present under the same idealization for each computation

Note first that the electron concentration gradient normal to the radome surface should be greater by at least one order of magnitude than the gradient parallel to the surface (in the case of a blunted cone, under the aerodynamic approximations, the gradient parallel to the surface vanishes) The natural approximation is thus to ignore this variation in discussing any axial location along the radome and include only the normal gradient As the normal gradient is severe, though, it must be considered Since the highly ionized zone and the radome proper may well lie within one or two vacuum wavelengths, it is probable that ray-tracing is an unacceptable procedure; a heterogeneous-layer reflection/transmission problem is apparently the simplest idealization that maintains most of the basic elements of the problem [11]

This idealization deletes a fundamental feature of the radome problem in ignoring the curvature of the surface, which may be appreciable relative to a wavelength, particularly near the stagnation point The only justification for this procedure lies in the heuristic argument that the curvature of the ionization sheath should introduce lesser-order effects than those derivable from a plane slab analysis, and since comparison is the means of interpreting the results, it is felt that the most important effect is adequately handled The region of the stagnation point is simply to be ignored as intractable at the present time

It is required to generate a procedure for solving the inhomogeneous slab problem which can be employed for arbitrary electron concentration and collision frequency distributions to sufficient accuracy to make valid comparisons as previously outlined The procedure suggested consists of approximating the equivalent dielectric constant profile by a series of closely spaced linear segments[12] and connecting the wave equation solutions at the endpoints ¶ This procedure is conceptually the simplest that maintains continuity of the electric field through the first derivative, and at the same time permits the evaluation of the expressions in some cases from tabulated complex functions [12 13] It is also well suited to digital computer implementation, as outlined in Appendix B The solution can be found for arbitrary angle of incidence and angle of polarization by superposition of the two special cases of polarization in and normal to the plane of incidence Using the forementioned idealization, consider first the case of a wave incident on the radome with an ionization sheath

¶It can be seen that this procedure is essentially identical to the numerical integration of the wave equation with a point by-point description of K (as performed in Ref 11)

Analysis of Incident Wave Case

Consider the laminated half-space $z \geq 0$ bounded by vacuum $z < 0$ To the depth z_0 exists a plama zone in which the dielectric constant is an arbitrary function of z Between z_0 and z_1 is a homogeneous slab of dielectric constant K_1, and it is bounded by a dielectric region $z > z_1$ of dielectric constant K_2 (ordinarily, but not necessarily, unity) Upon this structure, from the region $z < 0$, falls an electromagnetic wave (see Fig 1a) considered plane, propagating in a direction that makes an angle θ with the z axis (local normal) and having wave number k_0

The wave may be arbitrarily polarized Let α be the angle between the plane of the electric vector (plane containing **E** and the direction of propagation) and the plane of incidence (plane containing the normal and the direction of propagation) The incident electric vector of unit amplitude and (omitted) time dependence $\exp(-i\omega t)$ is given by

$$\mathbf{E}_{\text{inc}} = (\cos\alpha \cos\theta \mathbf{e}_x + \sin\alpha \mathbf{e}_y - \cos\alpha \sin\theta \mathbf{e}) \exp[ik_0(x \sin\theta + z \cos\theta)] \quad (12)$$

in a coordinate system in which $y = 0$ is the plane of incidence The fields existing in the homogeneous regions of space must be solutions to the two-dimensional Helmholtz equation:

$$\left(\frac{\partial^2}{\partial x^2} + \frac{\partial^2}{\partial z^2} + k_0^2 K\right) \mathbf{E} = 0 \quad (13)$$

where K is the dielectric constant of the medium The field in the inhomogeneous plasma zone satisfy more complex equations, here simplified by the superposition previously mentioned:

$$\mathbf{E} = E_y(x,z)\mathbf{e}_y + [i/\omega\epsilon_0 K(z)]\nabla \times [H_y(x,z)\mathbf{e}_y] \quad (14)$$

$$\mathbf{H} = H_y(x,z)e_y - (i/\omega\mu_0)\nabla \times [E_y(x,z)\mathbf{e}_y] \quad (15)$$

The component E_y and H_y waves satisfy, respectively,

$$\left[\frac{\partial^2}{\partial x^2} + \frac{\partial^2}{\partial z^2} + k_0^2 K(z)\right] E_y = 0 \quad (16)$$

$$\left[\frac{\partial^2}{\partial x^2} + \frac{\partial^2}{\partial z^2} - \frac{1}{K(z)}\frac{dK}{dz}\frac{\partial}{\partial z} + k_0^2 K(z)\right] H_y = 0 \quad (17)$$

The boundary conditions to be met are the continuity of E_x, E_y, H_x, and H_y, i e , the tangental components of **E** and $\nabla \times \mathbf{E}$

The foregoing equations are separated by solutions of the form required to match these boundary conditions, giving

$$(E_y,H_y) = [F(z),G(z)] \exp(ik_0 x \sin\theta) \quad (18)$$

$$\left\{\frac{d^2}{dz^2} + k_0^2[K(z) - \sin^2\theta]\right\} F_{1\,2} = 0 \quad (19)$$

$$\left[\frac{d^2}{dz^2} - \frac{1}{K}\frac{dK}{dz}\frac{d}{dz} + k_0^2(K - \sin^2\theta)\right] G_{1\,2} = 0 \quad (20)$$

where the subscripts 1 and 2 imply specific, linearly independent solutions:

$$F_1(0) = 1, F_1'(0) = 0 \qquad F_2(0) = 0, F_2'(0) = 1 \quad (21)$$

$$G_1(0) = 1, G_1'(0) = 0 \qquad G_2(0) = 0, G_2'(0) = 1 \quad (22)$$

Writing the reflected waves as

$$\mathbf{E}_r = (-R_2 \cos\alpha \cos\theta \mathbf{e}_x + R_1 \sin\alpha \mathbf{e}_y - R_2 \cos\alpha \sin\theta \mathbf{e}) \exp[ik_0(x \sin\theta - z \cos\theta)] \quad (23)$$

the transmitted wave as

$$\mathbf{E}_{tn} = [(T_2/K_2)(K_2 - \sin^2\theta)^{1/2} \cos\alpha \mathbf{e}_x + T_1 \sin\alpha \mathbf{e}_y - (T_2/K_2) \cos\alpha \sin\theta \mathbf{e}] \exp\{ik_0[x \sin\theta + z(K_2 - \sin^2\theta)^{1/2}]\} \quad (24)$$

and matching boundary conditions at $z = 0$, $z = z_0$, and $z = z_1$ by taking linear combinations of F_1 and F_2, and G_1 and G_2 gives rise to the following expressions for R_1, T_1, R_2, and T_2:

$$R_1 = -\frac{f_+'(z_0) - ik_0Q_1f_+(z_0)[(\gamma_{10}^2 - \gamma_{11}^2R_{12})/(\gamma_{10}^2 + \gamma_{11}^2R_{12})]}{f_-'(z_0) - ik_0Q_1f_-(z_0)[(\gamma_{10}^2 - \gamma_{11}^2R_{12})/(\gamma_{10}^2 + \gamma_{11}^2R_{12})]} \quad (25)$$

$$T_1 = \frac{-4ik_0 \cos\theta\gamma_{21}^{-1}\gamma_{11}\gamma_{10}[Q_1/(Q_1 + Q_2)]}{f_-'(z_0)(\gamma_{10}^2 + \gamma_{11}^2R_{12}) - ik_0Q_1f_-(z_0)(\gamma_{10}^2 - \gamma_{11}^2R_{12})} \quad (26)$$

$$R_2 = -\frac{g_+'(z_0) - ik_0Q_1[K(z_0)/K_1]g_+(z_0)[(\gamma_{10}^2 - \gamma_{11}^2R_{12}')/(\gamma_{10}^2 + \gamma_{11}^2R_{12}')]}{g_-'(z_0) - ik_0Q_1[K(z_0)/K_1]g_-(z_0)[(\gamma_{10}^2 + \gamma_{11}^2R_{12}')/(\gamma_{10}^2 + \gamma_{11}^2R_{12}')]} \quad (27)$$

$$T_2 = \frac{-4ik_0 \cos\theta K(z_0)\gamma_{21}^{-1}\gamma_{10}\gamma_{11}(K_2Q_1)/(K_1Q_2 + K_2Q_1)}{g_-'(z_0)(\gamma_{10}^2 + \gamma_{11}^2R_{12}') - ik_0Q_1[K(z_0)/K_1]g_-(z_0)(\gamma_{10}^2 - \gamma_{11}^2R_{12}')} \quad (28)$$

The shorthand notations employed are as follows:

$$f_\pm(z) = F_1(z) \pm ik_0 \cos\theta F_2(z)$$
$$g_\pm(z) = G_1(z) \pm ik_0K(0) \cos\theta G_2(z) \quad (29)$$

$$Q_{1,2} = (K_{1,2} - \sin^2\theta)^{1/2} \quad (30)$$

$$\gamma_{ij} = \exp(ik_0Q_iz_j) \quad (31)$$

$$R_{12} = (Q_1 - Q_2)/(Q_1 + Q_2) \quad (32)$$

$$R_{12}' = (K_2Q_1 - K_1Q_2)/(K_2Q_1 + K_1Q_2) \quad (33)$$

In deriving the foregoing expressions, use has been made of the Wronskian identity relevant to solution pairs (F_1,F_2) and (G_1,G_2) The specification of the reflected and transmitted waves, then, consists of solving the propagation equations, Eqs (19) and (20), for the functions f_+, f_-, g_+, and g_- with the boundary conditions

$$f_\pm(0) = 1 \qquad f_\pm'(0) = \pm ik_0 \cos\theta \quad (34)$$

$$g_\pm(0) = 1 \qquad g_\pm'(0) = \pm ik_0K(0) \cos\theta \quad (35)$$

The implementation of the solution under the approximation just outlined is illustrated in Appendix B

Emergent Wave Case

To solve the inverse problem, i e , the case of radiation from the radome, it is possible to use the formal result just obtained by solving an artificial problem as follows: assume there exists a slab of dielectric material of thickness z_3 and dielectric constant K_3, separated from the structure described previously by a vacuum gap of thickness z_4 as shown in Fig 1b Now let a plane wave be incident on this composite structure, and solve the reflection/transmission problem, making use of the fact that the ratio of the backward- to the forward-going wave at the plasma surface is equal to the reflection coefficient for the previous case When the problem is so expressed, the vacuum gap z_4 can be equated to zero The results of this procedure are new values for R_1, R_2, T_1, and T_2 (denoted with primes below) corresponding to a problem in which the plasma is "sandwiched" between two dielectric slabs If now the old R_1, R_2, T_1, and T_2 are evaluated for the case $K_1 = K_2 = 1$, with the plasma properties profiles inverted (denoted with superscripts zero below), the emergent wave problem is approximated

For the case of polarization normal to the plane of incidence there results

$$R_1' = \frac{R_1^0(\gamma_{33}^2 - R_{03}^2) + R_{03}(1 - \gamma_{33}^2)}{1 - \gamma_{33}^2R_{03}^2 - R_1^0R_{03}(1 - \gamma_{33}^2)} \quad (36)$$

$$T_1' = \frac{T_1^0\gamma_{33}(1 - R_{03}^2)}{1 - \gamma_{33}^2R_{03}^2 - R_1^0R_{03}(1 - \gamma_{33}^2)} \quad (37)$$

in the previous notation, where

$$R_{03} = (\cos\theta - Q_3)/(\cos\theta + Q_3) \quad (38)$$

For polarization in the plane of incidence, the coefficients are found to be

$$R_2' = \frac{R_2^0(\gamma_{33}^2 - R_{03}'^2) + R_{03}'(1 - \gamma_{33}^2)}{1 - \gamma_{33}^2R_{03}'^2 - R_2^0R_{03}'(1 - \gamma_{33}^2)} \quad (39)$$

$$T_2' = \frac{T_2^0\gamma_{33}(1 - R_{03}'^2)}{1 - \gamma_{33}^2R_{03}'^2 - R_2^0R_{03}'(1 - \gamma_{33}^2)} \quad (40)$$

where for this case

$$R_{03}' = (K_3 \cos\theta - Q_3)/(K_3 \cos\theta + Q_3) \quad (41)$$

and, of course,

$$Q_3 = (K_3 - \sin^2\theta)^{1/2} \quad (42)$$

Note that Eq (23) is formally correct whether or not the R's are decorated with prime superscripts, and the plane $z = 0$ is the origin of phase Equation (24) is also formally correct but should be multiplied by the factor $\exp(ik_0Q_2z_3)$ to obtain a common phase reference plane at $z = 0$, the surface of incidence

Interpretation of Results

Evaluation of receiving radome performance requires interpretation of the forementioned results in a consistent manner The method suggested for this purpose is the

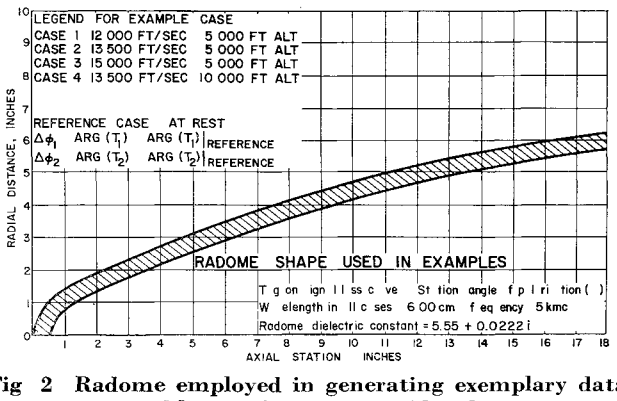

Fig 2 Radome employed in generating exemplary data and legend for cases considered

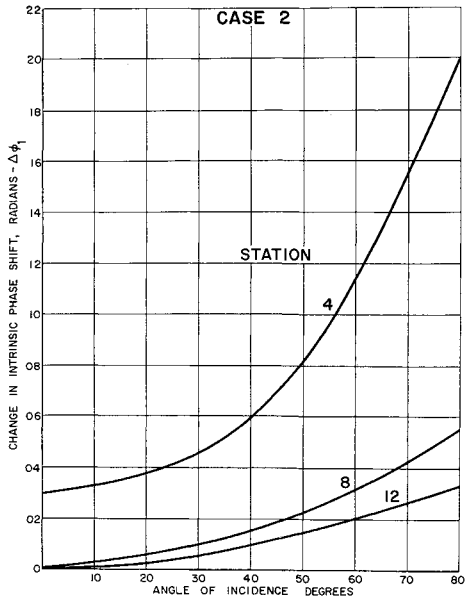

Fig 3 Change in intrinsic phase shift because of plasma layer: $\Delta\phi_1$ is arg(T_1)-arg(T_1)/reference, $\Delta\phi_2$ is arg(T_2)-arg(T_2)/reference

comparison of the intrinsic phase shift of the transmitted wave with the plasma sheath present with the phase shift of the transmitted wave due to the radome structure alone The difference is a measure of the phase distortion introduced by the plasma sheath Of course, this phase distortion will vary from station to station and with the angle of wave propagation with respect to the radome axis, as the plasma distribution and the angle of wave propagation with respect to the local normal varies The example radome profile Fig 2 illustrates this variation

If the "additional boresight error" is to be deduced, this is in principle merely a matter of geometry once the data already outlined has been generated More characteristically, however, it is required only to deduce the velocity-vs-altitude profile for which significant "additional boresight error" would be introduced for a given structure This profile can readily be decided by qualitative examination of the raw data from the electromagnetic calculations The exemplary data included here (Figs 3–8) reveal that the velocity-altitude boundary so defined is sufficiently sharp to permit this subjective mode of evaluation Case 1 (see Fig 2) showed no significant phase shifts

The forementioned considerations are, of course, based on the assumption of a phase-sensitive direction finder If,

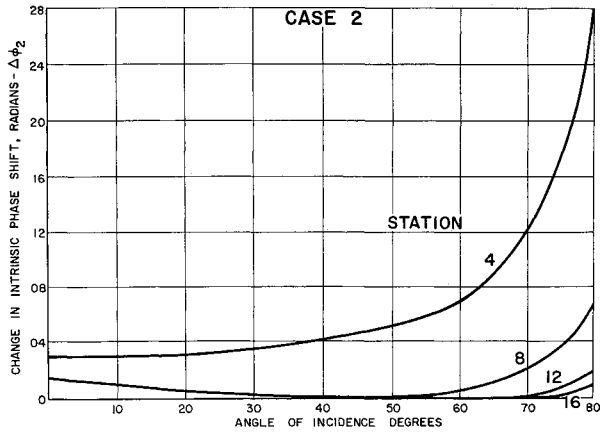

Fig 4 Change in intrinsic phase shift because of plasma layer: $\Delta\phi_1$ is arg(T_1)-arg(T_1)/reference, $\Delta\phi_2$ is arg(T_2)-arg(T_2)/reference

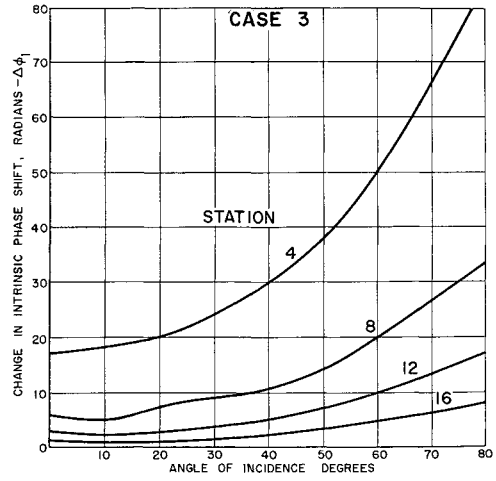

Fig 5 Change in intrinsic phase shift because of plasma layer: $\Delta\phi_1$ is arg(T_1)-arg(T_1)/reference, $\Delta\phi_2$ is arg(T_2)-arg(T_2)/reference

instead, the distribution of power flux is used as a means of direction fixing, then the one-way attenuation distribution is more important than the phase distortion The effect of polarization on one-way attenuation is attributable largely to the high dielectric constant of the radome and the concommitant reflection coefficient, as reference to the comparison Fig 9 (no plasma present) shows; this distribution on a "typical" radome is illustrated for several flight conditions in the accompanying Figs 10–12 It can be concluded that, in general, a phase-sensitive device will suffer greater degradation at lower speed than a hypothetical purely power-dependent system Case 1 was identical to the reference case and so is not plotted here

No attempt is made here to define a specific trajectory along which intolerable degradation would occur, since the criterion for acceptable radome performance depends upon the specific guidance scheme

Appendix A

In attempting to mechanize the aerodynamic calculations outlined previously, the greatest difficulty stems from the necessity of generating thermodynamic properties of air on the digital computer Fortunately, Grabau's formulation[10] permits a rapid implementation of these computations in the form of subroutines that provide values for h, s, Z, T, a, and γ as functions of P and ρ The functions actually

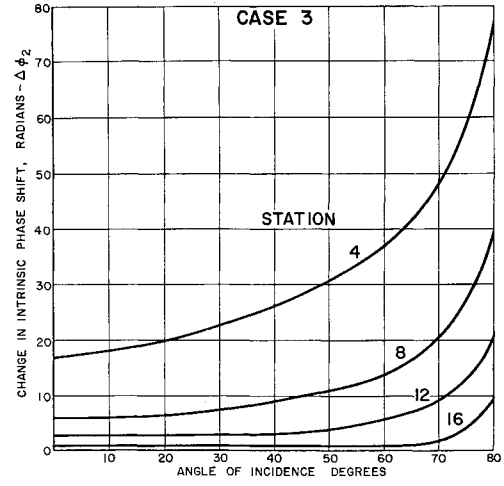

Fig 6 Change in intrinsic phase shift because of plasma layer: $\Delta\phi_1$ is arg(T_1)-arg(T_1)/reference, $\Delta\phi_2$ is arg(T_2)-arg(T_2)/reference

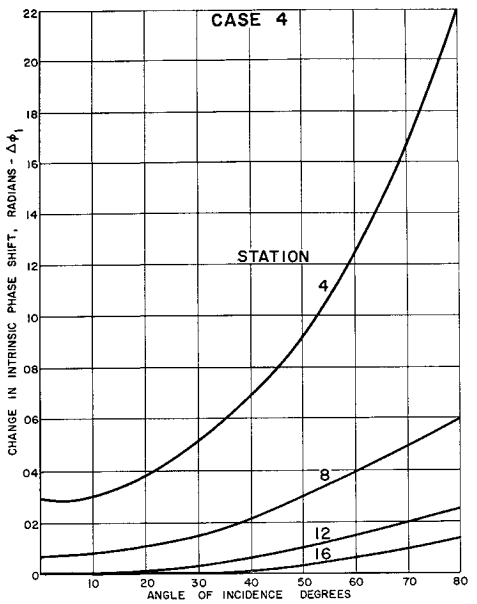

Fig 7 Change in intrinsic phase shift because of plasma layer: $\Delta\phi_1$ is arg(T_1)−arg(T_1)/reference, $\Delta\phi_2$ is arg(T_2)−arg(T_2)/reference

programmed are H_f, S_R, and Z, where

$$H_f = H\rho/P = H/ZRT \tag{A1}$$

$$S_R = S/R \tag{A2}$$

and the arguments are log$P$ and logρ With these functions and Z available, the other properties are easily derived:

$$\gamma = \rho a^2/P = (\partial \ln P/\partial \ln \rho) \tag{A3}$$

$$T = P/\rho RZ \tag{A4}$$

The oblique shock wave is handled by iteration of the Hugoniot equations in the following form:

$$\rho_1/\rho_2^{(n)} = \lambda^{(n)} \tag{A5}$$

$$P_2^{(n)} = [1 + \gamma_1 M_{1n}^2(1 - \gamma^{(n)})]P_1 \tag{A6}$$

$$\lambda^{(n+1)} = \frac{1 + [(\gamma_1 - 1)/2]M_{1n}^2[1 - (\lambda^{(n)})^2]}{1 + \gamma_1 M_{1n}^2(1 - \lambda^{(n)})} \frac{H_f(P_1,\rho_1)}{H_f(P_2^n,\rho_2^n)} \tag{A7}$$

using an initial value of λ given by the perfect-gas relation:

$$\lambda^{(0)} = \frac{2 + (\gamma - 1)M_{1n}^2}{(\gamma + 1)M_{1n}^2} \tag{A8}$$

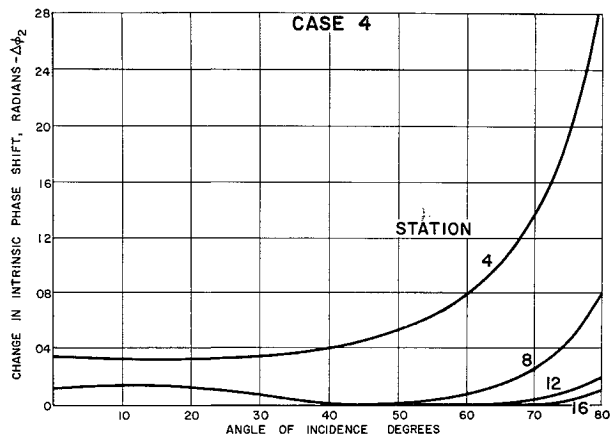

Fig 8 Change in intrinsic phase shift because of plasma layer: $\Delta\phi_1$ is arg(T_1)−arg(T_1)/reference, $\Delta\phi_2$ is arg(T_2)−arg(T_2)/reference

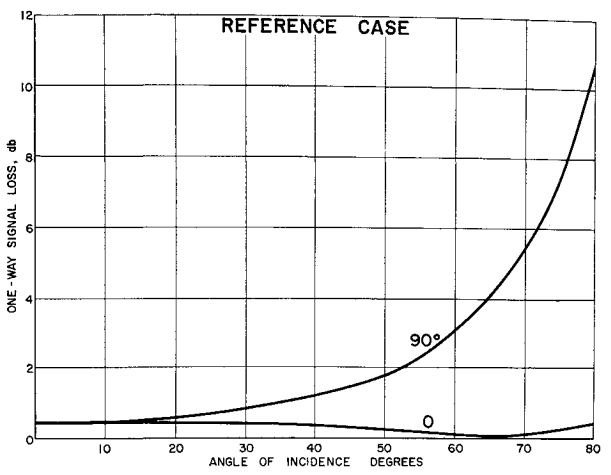

Fig 9 Attenuation because of radome alone

The angle of deflection of a streamline α' is given in terms of the shock angle θ :

$$\alpha' = \theta_s - \tan^{-1}(\lambda \tan\theta) \tag{A9}$$

Isentropic expansion can be handled a number of ways; the method used for the generation of the exemplary data here is an iteration of the equations

$$\Delta S_R^{(n)} = S_R(P_1,\rho_1) - S_R(P_2,\rho_2^{(n)}) \tag{A10}$$

$$\rho_2^{(n+1)} = \rho_2^{(n)} \exp\left(-\frac{\gamma^{(n)} - 1}{\gamma^{(n)}} \Delta S_R^{(n)}\right) \tag{A11}$$

using again an initial value given by the perfect-gas relation:

$$\rho_2^{(0)} = \rho_1(P_2/P_1)^{\gamma 1} \tag{A12}$$

With these operations available as subroutines, implementing the streamline calculations is a trivial task The air properties functions and the forementioned computations were coded in FORTRAN for IBM 7090, and the resulting program mapped 20 streamlines over five stations on a typical body in less than one minute

Appendix B

The approximate integration of Eqs (19) and (2) with boundary conditions (34) and (35) is required Under the linear segment approximation the equations can be put in the following form:

$$(d^2f/du^2) + (a + bu)f = 0 \tag{B1}$$

$$(c + du)(d^2g/du^2) - d(dg/du) + (a + bu)(c + du)g = 0 \tag{B2}$$

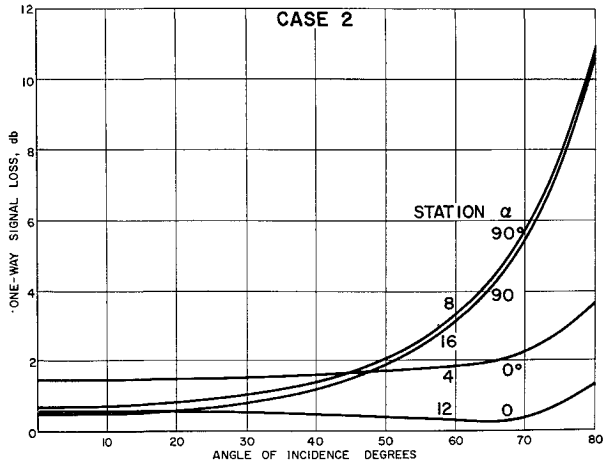

Fig 10 Attenuation through radome with plasma sheath; incident wave case

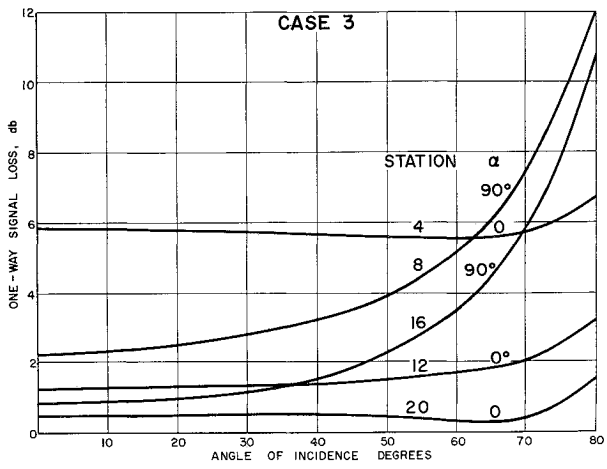

Fig 11 Attenuation through radome with plasma sheath; incident wave case

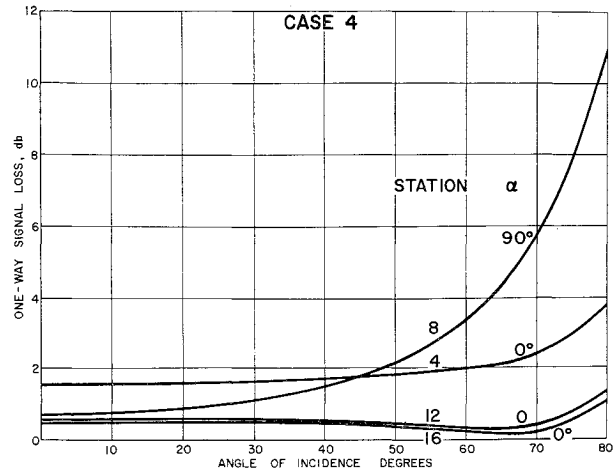

Fig 12 Attenuation through radome with plasma sheath; incident wave case

where

$$a = (K_i - \sin^2\theta)k_0^2(z_{i+1} - z_i)^2 \tag{B3}$$

$$b = (K_{i+1} - K_i)k_0^2(z_{i+1} - z_i)^2 \tag{B4}$$

$$c = K_i \tag{B5}$$

$$d = K_{i+1} - K_i \tag{B6}$$

$$u = (z - z)/(z_{i+1} - z_i) \tag{B7}$$

with the equations valid in the region $z_i \leq z \leq z_{i+1}$, in which region the dielectric constant changes linearly from K_i to K_{i+1}

There seems to be little virtue in putting the equations in a more standard form or expressing results in "closed" form if machine calculations are to be invoked in any event Therefore, power series solutions are obtained immediately:

$$f_\pm = \sum_0^\infty \alpha_n{}^\pm u^n \tag{B8}$$

$$g_\pm = \sum_0^\infty \beta_n{}^\pm u^n \tag{B9}$$

$$\alpha_0{}^\pm = f_\pm(z = z_i) \qquad \alpha_1{}^\pm = (z_{i+1} - z_i)(df_+/dz)_{z=i}$$
$$\alpha_2{}^\pm = -a\alpha_0{}^\pm/2 \tag{B10}$$

$$\alpha_n{}^\pm = -(a\alpha_{n-2}{}^\pm + b\alpha_{n-3}{}^\pm)/[n(n-1)] \tag{B11}$$

$$\beta_0{}^\pm = g^\pm(z = z_i) \qquad \beta_1{}^\pm = (z_{i+1} - z_i)(dg_\pm/dz)_{=i} \tag{B12}$$

$$\beta_2{}^\pm = \frac{\beta_1{}^\pm(d/c) - a\beta_0{}^\pm}{2} \qquad \beta_3{}^\pm = -\frac{a\beta_1{}^\pm + (b + ad/c)\beta_0{}^\pm}{6}$$

$$\beta_n{}^\pm = -\left[\frac{n-3}{n}\frac{d}{c}\beta_{n-1}{}^\pm + \frac{a}{n(n-1)}\beta_{n-2}{}^\pm + \frac{(b + ad/c)\beta_{n-3}{}^\pm}{n(n-1)} + \frac{db}{c}\frac{\beta_{n-4}{}^\pm}{n(n-1)}\right] \tag{B13}$$

The derivatives of these functions are obtained from similar series:

$$\frac{df_\pm}{dz} = (z_{i+1} - z_i)^{-1}\sum_0^\infty \gamma_n{}^\pm u^n \tag{B14}$$

$$\frac{dg_\pm}{dz} = (z_{i+1} - z_i)^{-1}\sum_0^\infty \delta_n{}^\pm u^n \tag{B15}$$

$$\gamma_0{}^\pm = 0 \qquad \gamma_1{}^\pm = (z_{i+1} - z_i)\left(\frac{df_\pm}{dz}\right) \tag{B16}$$

$$\gamma_2{}^\pm = -af_\pm(z = z_i) \qquad \gamma_3{}^\pm = \frac{-a\gamma_1{}^\pm + bf_\pm(z = z_i)}{2}$$

$$\gamma_n{}^\pm = \frac{[(a\gamma_{n-2}{}^\pm)/(n-2)] + [(b_{n-2}{}^\pm)/(n-3)]}{n-1} \tag{B17}$$

$$\delta_0{}^\pm = 0 \qquad \delta_1{}^\pm = (z_{i+1} - z_i)\left(\frac{dg_\pm}{dz}\right)_{=i}$$

$$\delta_2{}^\pm = \frac{d}{c}\delta_1{}^\pm - ag_\pm(z_i)$$

$$\delta_3{}^\pm = a\delta_1{}^\pm + \frac{[(bc + ad)/c]g_\pm(z = z_i)}{2}$$

$$\delta_4{}^\pm = -(d/c)\delta_3{}^\pm + a(\delta_2{}^\pm/2) + (bc + ad/c)\delta_1{}^\pm + (db/c)g_\pm(z = z_i) \tag{B18}$$

$$\delta_n{}^\pm = -\left[\frac{n-3}{n-1}\frac{d}{c}\delta_{n-1}{}^\pm + \frac{a\delta_{n-2}{}^\pm}{(n-1)(n-2)} + \frac{(b + ad/c)\delta_{n-3}{}^\pm}{(n-1)(n-3)} + \frac{db}{c}\frac{\delta_{n-4}{}^\pm}{(n-1)(n-4)}\right] \tag{B19}$$

The results are left in terms of recursion formulas since they are the most desirable expressions for computing application, and in practice the z_i's and k_0 should be made nondimensional by z_0 to avoid any possibility of error caused by units being inconsistent With these formulas one merely inserts the initial values of f, df/dz, g, and dg/dz from Eqs (34) and (35), the "constants" a, b, c, and d, and the geometrical factors $(z_{i+1} - z_i)/z_0$ for each plasma zone data point and proceeds to sum the resulting sequences Continuity of f, g, df/dz, and dg/dz provides the connecting relations between zones Note that all the series are bounded by geometric progressions Convergence is usually quite rapid; indeed an efficient IBM 7090 FORTRAN-compiled program carried out the outlined calculations using 20 data points and evaluated R_1, R_2, T_1, and T_2 at the rate of approximately 15 cases/min Single precision complex algebra was used throughout the program

References

[1] Chernyi G G , *Introduction to Hypersonic Flow,* transl by R F Probstein (Academic Press Inc , New York, 1961), Chaps II, IV, and V; also Hayes, W D and Probstein, R F , *Hypersonic Flow Theory* (Academic Press Inc , New York, 1959), Chaps IV–VI

[2] Deissler, R G and Loeffler, A L , Jr , "Analysis of turbulent flow and heat transfer on a flat plate at high Mach numbers with variable fluid properties, ' NASA TR R-17 (1959)

[3] Yakura, J K , "Theory of entropy layers and nose bluntness in hypersonic flow," *ARS Progress in Astronautics and Rocketry: Hypersonic Flow Research,* edited by F R Riddell (Academic Press Inc , New York, 1962), Vol 7, pp 421–470

[4] Seiff, A and Whiting, E E, "A correlation study of the bow wave profiles of blunt bodies," NASA TN D-1148 (February 1962)

[5] Witliff, C E and Curtis, J T, "Normal shock wave parameters in equilibrium air," Cornell Aeronaut Lab Rept CAL-111 (November 1961)

[6] Gray, J D, "Drag and stability derivatives of missile components according to the modified Newtonian theory," Arnold Eng Dev Center AEDC TN-60-191 (November 1960)

[7] Moeckel, W E and Weston, K C, "Composition and thermodynamic properties of air in chemical equilibrium," NACA TN 4265 (April 1958)

[8] Seiff, A and Whiting, E E, "Calculation of flow fields from bow-wave profiles for the downstream region of blunt-nosed circular cylinders in axial hypersonic flight," NASA TN D-1147 (November 1961)

[9] Molmud, P, "The electrical conductivity of weakly ionized gases," ARS Preprint 2586-62 (October 1962)

[10] Grabau, M, "A method of forming continuous empirical equations for the thermodynamic properties of air from ambient temperatures to 15,000°K with applications," Arnold Eng Dev Center AEDC-TN-59 102 (August 1962)

[11] Swift, C T and Evans, J S, "Generalized treatment of plane electromagnetic waves passing through an isotropic inhomogeneous plasma slab at arbitrary angles of incidence," NASA TR-R-172 (1963)

[12] Gold, R R, 'Reflection and transmission of electromagnetic waves from inhomogeneous magnetoactive plasma slabs," Aerospace Corp Rept TDR-169 (3230-11) TN-12 (March 1963)

[13] Albini, F A and Jahn, R G, "Reflection and transmission of electromagnetic waves at electron density gradients," J Appl Phys **32**, 75–82 (1961)

MARCH 1964 AIAA JOURNAL VOL 2, NO 3

Fluid Transpiration through Anodic Boundary of an Electric Arc

C SHEER,* J A COONEY,† AND D L ROTHACKER‡
Vitro Laboratories, West Orange, N J

Consideration of the distribution of dissipated energy in a free-burning arc indicates that the major portion of the input energy is concentrated at the anode-gas interface This leads to the concept of introducing a working fluid into the arc via the anodic boundary by transpiration through a porous anode Using porous graphite of sufficiently fine pore size and an inert gas medium, this technique is shown to be successful in generating a sustained plasmajet without a water-cooled channel or other thermal constraint At power levels <10 kw, energy transfer to the gas is in the range 70 8 to 88 5% of input The observed effects of gas flow on arc terminal characteristics are a rise in anode fall voltage and a decrease in incremental arc resistance Evidence for an apparent transition in anode fall mechanism at a specific flow rate is also presented Transient voltage probe studies of the flame reveal a complex structure for the axial potential distribution in the region of the anode

I Introduction

THE use of an electric arc as a primary energy source for heating streams of fluids has stimulated investigations of the basic energy transfer mechanisms occurring within the gas discharge zone Whereas the literature is replete with articles on the energetics and processes of the stationary arc discharge,[1] the behavior of an arc under forced convection of a fluid stream has received relatively scant attention despite its importance in the field of plasma generation The work reported thus far in this area has dealt largely with the technique of generating plasmajets, which involves passing a stream of fluid through the arc column As shown by the original work of Gerdien and Lotz[2] and later by Maecker[3] and others,[4 5] the concentration of appreciable amounts of enthalpy in the effluent jet requires the application of constraints on the column boundary This is accomplished by enveloping the column with a vortex of working fluid (the "vortex-stabilized" arc) or by establishing the column in a narrow channel with cooled walls (the "wall-stabilized" arc) In either case the conduction column is immobilized by thermal constriction with respect to radial displacement, thus permitting the convection of fluid through the hot plasma in the column without causing instability or flame-out

The use of this technique as a research tool in high-temperature science has become commonplace For some purposes, however, this method of heating fluids has some limitations For example, except at very low flow rates, the plasmajet is turbulent At low flow rates, on the other hand, problems are encountered in sustained operation with regard to electrode erosion and contamination of the jet, unless the arc is operated at relatively low power

The present paper is concerned with a new method of energizing a stream of fluid by means of an electric arc without the application of thermal constraints on the arc column

Received September 17, 1963; revision received January 21, 1964 The work reported in this paper was performed at Vitro Laboratories, West Orange, N J, during the period August 1958 to July 1961 when all three authors were staff members of the Arc Research Department The research was cosponsored by the Mechanics Branch of the Air Force Office of Scientific Research and the Thermomechanics Research Laboratory of the Aeronautical Research Laboratory under Air Contract No AF 49(638)-477

* Now Senior Staff Scientist, Electronics Research Laboratories, Columbia University, New York, N Y

† Now Senior Engineer, Astro Electronics Division, Radio Corporation of America, Camden, N J

‡ Now Senior Research Engineer, Electronics Research Laboratories, Columbia University, New York, N Y